PAPER

Check for updates

Elimination mechanism of vanillin from non-phenolic β-O-4-type terminals formed in guaiacyl lignin: a combined kinetic and theoretical study

Yuki Hirano, [ID] [a] Haruhiko Fukaya,[b] Tsunehisa Miki,[b] Takashi Hosoya [ID] *[a] and Hisashi Miyafuji [ID] [a]

The alkaline aerobic oxidation of lignin to vanillin (4-hydroxy-3-methoxybenzaldehyde) has been employed as an industrial method for producing bio-based low-molecular-weight aromatic compounds. To deepen the molecular-level understanding of this reaction, we have been investigating the vanillin formation mechanism from native softwood lignin. One of the major reaction pathways involves oxidative degradation of β-O-4-type internal units, followed by alkaline-induced elimination of vanillin from the resulting vanillin end group. This study examined the reaction mechanism of a model compound, 4-[2-(3-ethoxy-4-methoxyphenyl)-2-hydroxy-1-(hydroxymethyl)ethoxy]-3-methoxybenzaldehyde, VE_β, which mimics the vanillin end group, in 4.0 mol L^{-1} aqueous NaOH, with particular focus on the formation pathways of vanillin and byproducts. VE_β rapidly formed an equilibrium mixture comprising various rearranged compounds, in which the vanillin residue had migrated to the α- and γ-positions of the side-chain via an acetal-type intermediate. Kinetic analysis based on a pseudo-first-order competitive reaction model revealed that this equilibrium mixture was consumed through two distinct pathways: vanillin elimination and side reaction accompanied by polymerization. The activation energy (E_a) for vanillin elimination was determined to be 17.0 kcal mol^{-1}, which agreed moderately with the E_a value of 20.7 kcal mol^{-1} calculated by DFT(M06-2X) for the α-oxyanion-assisted elimination process. Although the details of the side reaction pathway remain unclear, the overall reaction followed pseudo-first-order kinetics despite the involvement of bimolecular steps, suggesting that the rate-determining step of the side reaction proceeds via a unimolecular process.

Introduction

Lignin is an aromatic polymer that constitutes approximately 15–35 wt% of lignocellulose.[1] Various methods for depolymerizing lignin into low-molecular-weight aromatic compounds useful for the chemical industry have been investigated.[2–10] Among these methods, alkaline aerobic oxidation is considered promising due to its use of non-toxic molecular oxygen as the oxidant. This method enables the effective cleavage of the major interunit linkages in lignin, particularly ether bonds, leading to the oxidative degradation of the C_3 side-chains and the production of low-molecular-weight phenols.[11–21]

The alkaline aerobic oxidation method has already been industrialized as a means of producing vanillin from lignosulfonates, which are byproducts of the sulfite pulping process of softwood.[2,22–24] Vanillin (4-hydroxy-3-methoxybenzaldehyde) is

not only used as a flavoring agent but also serves as a key chemical intermediate in the synthesis of pharmaceuticals and other industrial chemicals.[24] The industrial production of vanillin from lignosulfonates involves oxidative degradation under pressurized air at around 170 °C using Cu^{2+} as a catalyst, and this method was the dominant process for global vanillin production until the 1980s. However, this process has major drawbacks, including low vanillin yields (typically below 10 wt%) and the difficulty of isolating vanillin from the reaction mixture.[25] As a result, petroleum-based processes have become the mainstream approach. Nevertheless, in light of growing environmental awareness, the revival of lignin-based vanillin production is of considerable significance.

To improve the production process of vanillin from lignin, numerous studies have aimed to increase the yield of vanillin by enhancing reaction efficiency through various catalysts and optimizing the process from a chemical engineering perspective.[22,26–32] In contrast, only a limited number of studies have addressed the reaction mechanism of vanillin formation from lignin during alkaline aerobic oxidation. The degradation mechanism of lignin by molecular oxygen has been investigated in detail primarily from the perspective of pulp bleaching,

[a]Graduate School of Life and Environmental Sciences, Kyoto Prefectural University, Japan. 1-5 Shimogamo-hangi-cho, Sakyo-ku, Kyoto 606-8522, Japan. E-mail: hosoya_t@kpu.ac.jp

[b]Multi-Material Research Institute, National Institute of Advanced Industrial Science and Technology (AIST), 4-205 Sakurazaka, Moriyama-ku, Nagoya 463-8560, Japan
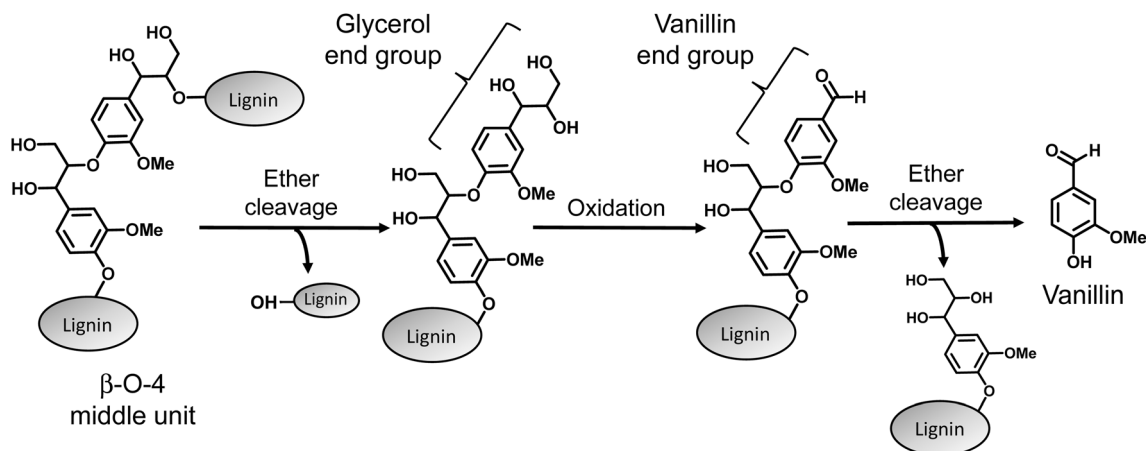
Scheme 1 Vanillin production pathway from a β-O-4 middle unit of lignin during alkaline aerobic oxidation.[39–41]

rather than from the standpoint of chemical production from lignin. In such studies, the main focus has been on the degradation of benzene ring structures within lignin that contribute to color formation, while the oxidative conversion of lignin side-chains into vanillin has been regarded as a side reaction.[33–38] Thus, although the bleaching mechanisms proposed in previous studies deal with the same fundamental phenomenon—namely, the degradation of lignin by molecular oxygen under alkaline conditions—their focus differs significantly. As a result, they cannot be directly referenced as rational guidelines for controlling the vanillin production process.

Against this background, we have undertaken a study aimed at elucidating the mechanism of vanillin formation during the alkaline aerobic oxidation of lignin, with the goal of acquiring microscopic insights into the oxidative reactions that can be utilized for the development and control of vanillin production processes. Our previous research has focused on intermediate

structures containing the β-O-4 linkage—a major type of linkage found in lignin—and has proposed a vanillin formation pathway as illustrated in Scheme 1.[39–41] In this pathway, the β-ether bond undergoes non-oxidative cleavage under alkaline conditions to generate a glycerol end group. The side-chain of this end group is then oxidized to form a vanillin end group. Subsequently, the β-ether bond adjacent to this unit is cleaved non-oxidatively under alkaline conditions, resulting in the release of a vanillin molecule.

This study focuses on the final step depicted in Scheme 1—namely, the non-oxidative elimination of a vanillin molecule from a vanillin end group. The present series of investigations was conducted as a continuation of our previous work.[42] The reaction behavior of a model compound representing the vanillin end group structure, 4-[2-(3-ethoxy-4-methoxy-phenyl)-2-hydroxy-1-(hydroxymethyl)ethoxy]-3-methoxy-benzaldehyde, **VE$_β$**, under typical alkaline conditions (aqueous 4.0 mol L^{-1}
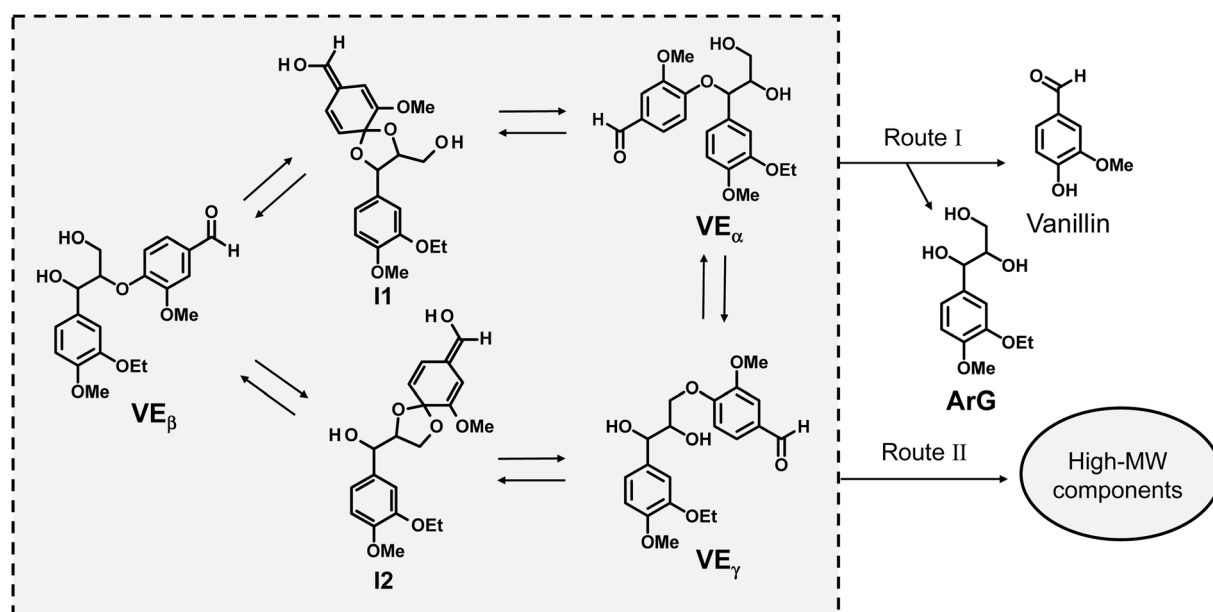
Scheme 2 Reaction pathways proceeding from **VE$_β$** proposed in our previous study.[42]

NaOH), as shown in Scheme 2, is of particular interest to both wood chemists and organic chemists. Specifically, under ambient alkaline conditions, VE_β rapidly establishes an equilibrium with two rearranged compounds—4-(1-(3,4-dimethoxyphenyl)-2,3-dihydroxypropoxy)-3-methoxybenzaldehyde, VE_α and 4-(3-(3,4-dimethoxyphenyl)-2,3-dihydroxypropoxy)-3-methoxybenzaldehyde, VE_γ—via acetal intermediates (**I1** and **I2**), in which the vanillin residue has migrated to the α- and γ-positions, respectively. Upon heating, this equilibrium mixture undergoes two main reactions: one is the cleavage of the ether bond to form vanillin and 1-(3-ethoxy-4-methoxy-phenyl) propane-1,2,3-triol, **ArG**, designated as Route I; the other is the formation of high-molecular-weight components (hereafter referred to as "High-MW components"), designated as Route II.

The above findings raise several new questions, among which a primary issue is the mechanism by which vanillin is eliminated in Route I. Two possible mechanisms have been proposed, as illustrated in Scheme 3. One is the S_NicB mechanism, in which a neighboring alkoxide attacks the ether linkage, leading to its cleavage. The other is the S_NAr mechanism, which involves a hydroxide ion attacking the aromatic carbon followed by cleavage of the ether bond.[37,43-45] Previous studies on model compounds with C_2 side-chains structurally similar to that of VE_β have reported results supporting the S_NicB mechanism, based on kinetic analysis and reaction behavior in ^{18}O-labeled aqueous media.[44] However, those findings were obtained under limited reaction conditions (dioxane-0.5 mol L^{-1} NaOH aqueous solution at 75 °C), and do not necessarily validate the applicability of the S_NicB mechanism under the more strongly alkaline conditions (∼4.0 mol L^{-1} NaOH) employed in our proposed vanillin production process. Furthermore, in prior kinetic analyses, the formation of High-MW components via Route II had not yet been recognized and was thus never included in kinetic considerations. Therefore, elucidating the detailed nature of Route II constitutes another new challenge that emerged from our previous study.

In this study, we employed VE_β—a model compound previously investigated by our group—as a representative vanillin end group, with the objective of gaining deeper mechanistic insights into its reaction behavior in aqueous 4.0 mol L^{-1} NaOH solution, beyond the reaction pathways illustrated in Scheme 2. In the first half of this paper, we construct a kinetic model based on the assumption of competitive degradation of VE_β via Route I and Route II (Scheme 2), and conduct a detailed kinetic analysis grounded in this model. This section is expected to provide mechanistic insights including activation parameters for both Route I and Route II. The formation mechanism of the High-MW components in Route II is also discussed based on the results of the kinetic analysis. In the latter half of the paper, theoretical calculations are performed to elucidate the molecular mechanism of vanillin elimination in Route I. In this part, we compare the activation barriers obtained experimentally with the calculated values and discuss the detailed mechanism of vanillin elimination.

## Experimental

Materials

Alkaline degradation and product analysis

An ethanol solution of VE_β with a precisely adjusted concentration was added to a perfluoroalkoxy alkane (PFA) test tube (total volume: 5.0 mL) so that the amount of the model compound introduced was 3.0 mg (7.97 μmol). After removing the solvent under reduced pressure, a magnetic stir bar was placed inside the tube. In a nitrogen-filled glove box, 2.0 mL of 4.0 mol L^{-1} aqueous sodium hydroxide solution was added to the tube, which was then sealed with a silicone stopper. The reaction was initiated by immersing the tube in an oil bath maintained at a temperature between 21 and 60 °C. After

S_NicB mechanism
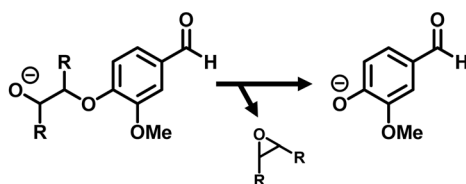
S_NAr mechanism
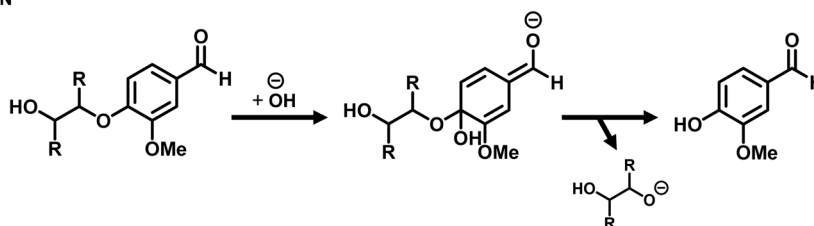
Scheme 3 S_NicB and S_NAr mechanisms for vanillin elimination.

stirring the mixture for 10 min to 4 h, the tube was removed, cooled, and opened. Then, 1.0 mL of ethanol containing exactly 1.0 mg of the internal standard compound (*p*-hydroxybenzaldehyde) was added to the reaction mixture. A 20 μL aliquot of the resulting solution was diluted with 980 μL of 0.08 mol L^{-1} aqueous trifluoroacetic acid/acetonitrile solution (9/1, v/v), filtered through a 0.45 μm syringe filter (quantity: 100 filters), and used as the sample for HPLC analysis.

HPLC analysis was performed using a system equipped with a Shimadzu LC-20AD pump, CTO-20AC column oven, and SPD-M40 photodiode array detector. The analytical conditions were as follows: Cadenza CD-C18 column (Imtakt), column temperature 35 °C, flow rate 0.8 mL min^{-1}, and a mobile phase gradient composed of 0.1% aqueous trifluoroacetic acid and acetonitrile, programmed as follows: 90/10 → 45/55 (0–30 min), 45/55 → 0/100 (30–35 min), 0/100 (35–40 min), 0/100 → 45/55 (40–45 min), and 45/55 → 90/10 (45–50 min). Quantification of the major substances in the reaction solution—vanillin, **ArG**, **VE**$_\alpha$, and **VE**$_\gamma$—was carried out by comparing the peak areas of each compound with that of the internal standard. Calibration curves were prepared by HPLC analysis of standard samples of the target products and the internal standard. For **ArG**, a calibration curve could not be directly prepared due to the difficulty in isolating a sufficient quantity; instead, the calibration curve for veratrylglycerol, which we previously examined, was used as a substitute.[46] Similarly, the calibration curves for **VE**$_\alpha$ and **VE**$_\gamma$ were substituted with that of **VE**$_\beta$.

Kinetic analysis

Kinetic analysis in this study was conducted based on the pseudo-first-order competitive reaction model shown in Scheme 4. In this model **VE**$_\alpha$, **VE**$_\beta$, **VE**$_\gamma$—three isomers that rapidly interconvert—are collectively defined as the starting substrates. From these substrates, two competing reactions occur: one leads to the formation of vanillin with a rate constant k_1, and the other leads to the formation of byproducts with a rate constant k_2. These competitive reactions are assumed to be significantly slower than the interconversion among the three substrates and are treated as irreversible. Although hydroxide ions are undoubtedly involved in the reaction, the experimental conditions involve a large excess of hydroxide ions relative to the substrate concentration. A pseudo-first-order approximation is therefore considered valid, treating [OH$^-$] as a constant.

In this model, the total concentration of the three starting substrates at reaction time t—namely [VE$_\beta$] + [VE$_\alpha$] + [VE$_\gamma$]—is expressed by the following eqn (1), using the overall rate constant k_T, which corresponds to the rate constant for the degradation of the starting materials.

$$\ln([VE_\beta] + [VE_\alpha] + [VE_\gamma]) = \ln([VE_\beta]_0 + [VE_\alpha]_0 + [VE_\gamma]_0) - k_T t \quad (1)$$

Here, [VE$_\beta$]$_0$, [VE$_\alpha$]$_0$, [VE$_\gamma$]$_0$ represent the initial concentrations of each starting compound. Since **VE**$_\alpha$ and **VE**$_\gamma$ are not present in the system at the beginning of the reaction, their initial concentrations are [VE$_\alpha$]$_0$ = [VE$_\gamma$]$_0$ = 0.

The concentration of vanillin, [Vanillin], at reaction time t in this model is described by the following eqn (2), which is the analytical solution of the differential equations corresponding to the competitive reaction model shown in Scheme 4.

$$[Vanillin] = k_1([VE_\beta]_0 + [VE_\alpha]_0 + [VE_\gamma]_0)(1 - e^{-k_T t})/k_T \quad (2)$$

From this equation, it can be seen that plotting ([VE$_\beta$]$_0$ + [VE$_\alpha$]$_0$ + [VE$_\gamma$]$_0$)(1 − $e^{-k_T t}$)/k_T against [Vanillin] yields a straight line with a slope of k_1.

The formation rate constant k_2 for the High-MW components can be determined using the following eqn (3).

$$k_2 = k_T - k_1 \quad (3)$$

An Arrhenius plot was constructed using the rate constants k obtained at each reaction temperature T. Based on the Arrhenius equation shown in eqn (4), the activation energy (E_a) and the frequency factor A were calculated from the slope and intercept of the regression line, respectively. Here, R denotes the universal gas constant.

$$\ln k = -\frac{E_a}{RT} + \ln A \quad (4)$$

The activation entropy ($\Delta S^\ddagger$) was calculated using the frequency factor A, Boltzmann constant k_B, Planck constant h, temperature T, and gas constant R, according to eqn (5) shown below.

$$\Delta S^\ddagger = R \ln \frac{hA}{e^2 k_B T} \quad (5)$$

Quantum chemical calculation

Quantum chemical calculations were performed using the GAUSSIAN 09 program package.[47] Geometry optimizations and frequency calculations were carried out using the DFT (M06-2X) method. For this method, the 6-31G basis set was used for hydrogen atoms, and the 6-31G(d) basis set was used for carbon and oxygen atoms. In addition, diffuse functions were added to the carbon and oxygen atoms, and p-type polarization functions were added to the hydrogen atoms in hydroxyl groups. This basis set is hereafter referred to as BS-I. Single-point energy calculations were performed on each optimized structure. For these calculations, the cc-pVTZ basis set was used for hydrogen atoms, and the aug-cc-pVTZ basis set was used for carbon and oxygen atoms. This basis set is referred to as BS-II. The potential energy was corrected using the zero-point energy obtained from the frequency calculations. Furthermore, the Gibbs free
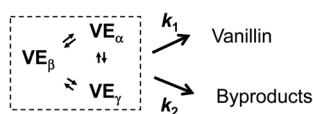
Scheme 4 Pseudo-first-order competitive reaction model used in this study, proceeding from an equilibrium mixture consisting of **VE**$_\beta$, **VE**$_\alpha$ and **VE**$_\gamma$.

energies of all structures were estimated by calculating the entropy and enthalpy at 298.15 K and 1 atm based on the vibrational analysis. We confirmed that all optimized equilibrium structures had no imaginary vibrational modes, and that each transition state structure had exactly one imaginary vibrational mode. The connectivity of each optimized transition state to its corresponding reactant and product was verified by visualizing the imaginary vibrational mode and performing intrinsic reaction coordinate calculations based on the steepest descent method.

Results and discussion

Degradation behavior of VE_β and its kinetic analysis

The degradation of VE_β in 4.0 mol L^{-1} aqueous NaOH was conducted at temperatures ranging from 21 to 60 °C. At all reaction temperatures, VE_α and VE_γ—rearranged products in which the vanillin residue of VE_β had migrated—were detected in the reaction solution shortly after the initiation of the experiment (see HPLC chromatogram in Fig. S1 in the SI). This observation confirms that the equilibrium among VE_α, VE_β, and VE_γ, as proposed in Scheme 2 in our previous study, was indeed established under all temperature conditions examined in the present work. Notably, at all reaction temperatures, the total recovery of VE_α, VE_β, and VE_γ in the early stage of the reaction was much higher than the yields of vanillin or **ArG** at the same time point (see Fig. S2 in the SI). This result clearly indicates that the interconversion among VE_α, VE_β, and VE_γ proceeds significantly faster than the subsequent formation of vanillin and **ArG**. Hereafter, VE_α, VE_β, and VE_γ are collectively referred to as the "starting materials (SMs)".

Table 1 summarizes the yields of vanillin and **ArG** at the longest reaction times employed at each temperature. In addition, changes with time in the recovery of the SMs and the yields of the main products during the reaction are provided in the SI (see Fig. S2). Vanillin was produced from the SMs with yields ranging from 22.4 to 63.4 mol%. At 50 °C, the yields of vanillin and **ArG**, which generally exhibited an increasing trend with temperature, showed a temporary decrease; however, this phenomenon is considered to arise from experimental error

associated mainly with the batch-type experiments employed in this study. When recalculated based on the amount of SMs degraded, these values correspond to approximately 40–65 mol%, indicating that the SMs did not convert to vanillin quantitatively at any of the tested temperatures. As we reported previously, the SMs also give rise to byproducts with relatively high molecular weights in addition to vanillin.[42] Although molecular weight measurements of the products were not performed in the present study, it is considered that similar High-MW components were formed as byproducts in the course of the reaction. Quantification of the high-molecular-weight components is not feasible due to the structural diversity involved, and therefore was not conducted in this study. Notably, the yield of **ArG** was consistently lower than that of vanillin. This observation will be revisited in the later discussion of the vanillin elimination mechanism.

Based on the above discussion, it is strongly suggested that the SMs, including VE_β, underwent degradation through two competing pathways at all temperature ranges: one leading to vanillin formation and the other to the formation of byproducts. To gain a deeper understanding of this observation, we carried out kinetic analyses from two perspectives—degradation of the SMs and formation of vanillin—based on the pseudo-first-order competitive reaction model shown in Scheme 4.

Semi-logarithmic plots of SMs concentration *versus* reaction time at 21–60 °C in Fig. 1A yielded linear relationships between the logarithm of SMs concentration and reaction time at all tested temperatures. This result indicates that eqn (1) holds under conditions with a large excess of hydroxide ions, and that the degradation of SMs can be approximated as a pseudo-first-order reaction. Similar pseudo-first-order kinetics have also been reported for lignin model compounds with C_2 side-chains analogous to VE_β, in which the vanillin residue acts as a leaving group, under alkaline conditions,[44,45,48] and the present results support this observation. Furthermore, as shown in Fig. 1B, a linear relationship was also observed between the vanillin concentration and the expression $([VE_\beta]_0 + [VE_\alpha]_0 + [VE_\gamma]_0)(1 - e^{-k_T t})/k_T$ (see eqn (2) in the Experimental section). This finding demonstrates that the pseudo-first-order competitive reaction model appropriately describes the degradation behavior of the SMs. In contrast, a semi-logarithmic plot of vanillin concentration *versus* reaction time did not yield a linear relationship (see Fig. S3 in the SI). This result further supports the notion—based on an independent line of evidence—that the degradation of SMs involves not only vanillin formation but also competing side reaction.

From the slopes of the plots in Fig. 1, the pseudo-first-order rate constants k_T and k_1 at each temperature were calculated, and the rate constant k_2 was subsequently obtained from the difference between k_T and k_1, according to eqn (3). As shown in Table 2, the overall rate constant k_T for the degradation of the SMs ranged from 5.8 to 110 (s^{-1} 10^{-5}). The rate constant k_1, corresponding to vanillin formation, ranged from 1.7 to 44.5 (s^{-1} 10^{-5}), while the rate constant k_2, which is considered to correspond to the formation of high-molecular-weight byproducts, ranged from 4.1 to 65.2 (s^{-1} 10^{-5}). A comparison of the two rate constants reveals that k_2 was consistently slightly greater

Table 1 Yields of vanillin and **ArG** and recovery of SMs after the degradation experiments in 4.0 mol L^{-1} NaOH aq. at various reaction temperatures under N_2

Temperature (°C)	Reaction time (min)	Recovery (%)[a]	Yield (mol%)	
			Vanillin	ArG
21	240	43.5	22.4 (39.7)[b]	10.2 (18.1)
30	180	32.4	35.1 (51.9)	21.4 (31.2)
40	120	15.1	48.1 (56.6)	34.8 (41.0)
50	90	20.9	41.7 (52.7)	29.4 (37.1)
60	60	1.6	63.4 (64.4)	52.7 (53.5)

[a] The recovery yield is presented as the total value of SMs (VE_β, VE_α and VE_γ). [b] The number in the parenthesis shows yields (mol%) of Vanillin or **ArG** on the basis of the degraded SMs (VE_β, VE_α and VE_γ).
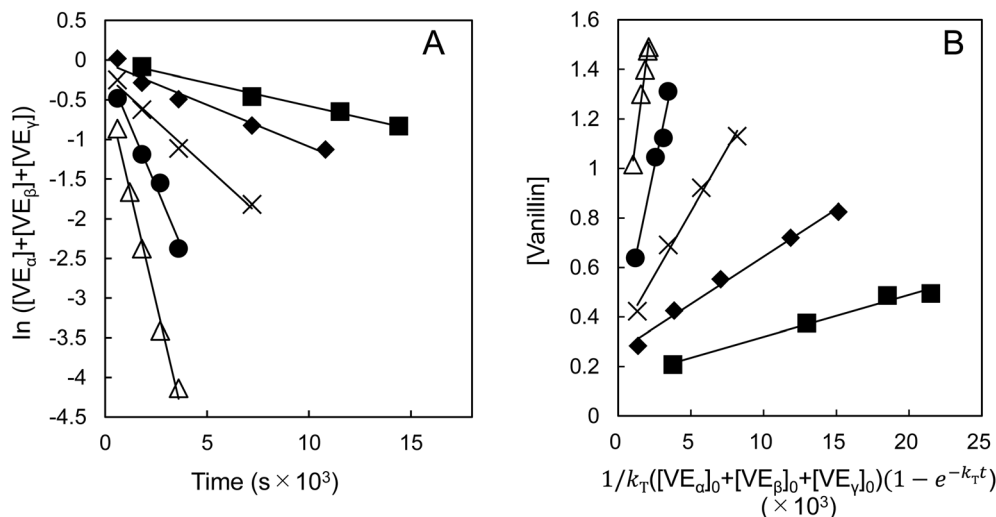
Fig. 1 Semi-logarithmic plot of the temporal changes in the reactant concentration during the degradation of SMs (A), and the plot of the vanillin concentration against $([VE_\beta]_0 + [VE_\alpha]_0 + [VE_\gamma]_0)(1 - e^{-k_\mathrm{T}t})/k_T$ (B), in 4.0 mol L^{-1} NaOH aq. at 21–60 °C under N$_2$. Reaction temperatures: 21 °C (■), 30 °C (◆), 40 °C (×), 50 °C (●), 60 °C (△). The coefficients of determination (R^2) of the linear fits are as follows: 21 °C (k_1: 0.982, k_T: 0.992); 30 °C (k_1: 0.940, k_T: 0.965); 40 °C (k_1: 0.992, k_T: 0.988); 50 °C (k_1: 0. 978, k_T: 0.978); 60 °C (k_1: 0.990, k_T: 0.992).

than k_1 at all reaction temperatures. This observation is not entirely consistent with the fact that, in some cases, the vanillin yields based on degraded SMs slightly exceeded 50 mol% (see Table 1). One possible explanation for this discrepancy is that intermediates capable of producing vanillin may be generated in the side reaction pathway (Route II) shown in Scheme 2. If this assumption is valid, the kinetic model presented in Scheme 4 does not fully reflect the actual degradation pathways of the SMs. This issue will likely be resolved in future research through the elucidation of more specific chemical processes involved in

the side reaction pathways, including the actual nature of intermediate **I**, and the adoption of a more refined kinetic model based on these findings. Nevertheless, given that the linear fit in Fig. 1B is excellent and that vanillin yields never significantly exceed 50 mol% at any temperature, we proceed with our discussion under the premise that the kinetic model shown in Scheme 4 remains a valid representation.

The kinetic analysis presented thus far provides important insights into the side reaction (Route II) other than vanillin formation. The formation of high-molecular-weight components, which are presumed to be products of Route II, undoubtedly involves molecular collisions between SMs or intermediates derived therefrom. On the other hand, it is noteworthy that the kinetic model shown in Scheme 4, which assumes a pseudo-first-order reaction with [OH$^-$] treated as constant, describes the degradation behavior of the SMs well. This observation strongly suggests that the collision-based steps in the side reaction pathway are not rate-determining. As illustrated in Scheme 5, it is therefore proposed that a highly reactive intermediate **I** is formed unimolecularly from the SMs, and that this step constitutes the rate-determining step of the side reaction. After the formation of **I**, subsequent reactions between these intermediates are presumed to lead to the generation of dimers or higher oligomers. Although the specific chemical identity of intermediate **I** (or a group of such intermediates) remains unclear at present, future studies using appropriately designed model compounds will be important to clarify their structural features and are expected to shed light on the molecular mechanism underlying this side reaction

Table 2 Pseudo-first order kinetic constants (k, s^{-1} × 10^{-5}) and activation parameters (kcal mol^{-1}), activation energy (E_a), activation enthalpy ($\Delta H^\ddagger$), activation entropy ($\Delta S^\ddagger$), and activation Gibbs energy ($\Delta G^\ddagger$) determined in the degradation of SMs under the conditions of 4.0 mol L^{-1} NaOH aq./N$_2$

	k_T	k_1	k_2
21 °C	5.8 ± 0.036[a]	1.7 ± 0.022	4.1 ± 0.042
30 °C	10.6 ± 0.096	3.8 ± 0.025	6.7 ± 0.099
40 °C	23.4 ± 0.089	10.3 ± 0.032	13.2 ± 0.095
50 °C	60.8 ± 0.145	28.2 ± 0.052	32.6 ± 0.154
60 °C	110 ± 0.135	44.5 ± 0.022	65.2 ± 0.136
Activation parameters			
E_a[b]	15.1	17.0	14.1
$\Delta H^\ddagger$	14.6 (19.6)[c]	16.4	13.5
$\Delta S^\ddagger$ (cal mol^{-1} K)[b]	−30.6 (−22)[c]	−26.6	−34.9
$\Delta G^\ddagger$ (kcal mol^{-1})[d]	23.7	24.3	23.9

[a] Standard error. [b] The activation energy and activation entropy were calculated according to the slope and intercept of the Arrhenius plot in Fig. 2, respectively. [c] Values in parentheses are taken from ref. 44. [d] The activation Gibbs energy, $\Delta G^\ddagger$, was calculated at 25 °C (T = 298.15 K) using the equation "$\Delta G^\ddagger = \Delta H^\ddagger - T\Delta S^\ddagger$" after determining the activation enthalpy, $\Delta H^\ddagger$, from the activation energy, E_a, using the equation "$\Delta H^\ddagger = E_a - RT$".
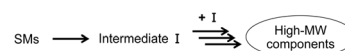
Scheme 5 Schematic illustration of processes involved in Route II.

pathway. Nevertheless, the above findings imply that suppressing the formation or accumulation of intermediate **I** could be an effective strategy to minimize polymerization and thereby improve vanillin yields under alkaline conditions.

An Arrhenius plot was constructed from the logarithm of the rate constant k at each temperature listed in Table 2 *versus* the reciprocal of the reaction temperature T. As shown in Fig. 2, linear relationships were obtained for all cases: k_T (degradation of SMs), k_1 (vanillin formation), and k_2 (side reactions). From the slopes and intercepts of the resulting regression lines, various activation parameters were calculated according to eqn (4) and (5). The activation energy (E_a), activation enthalpy ($\Delta H^{\ddagger}$), and activation entropy ($\Delta S^{\ddagger}$) derived from k_T were 15.1 kcal mol^{-1}, 14.6 kcal mol^{-1}, and −30.6 cal mol^{-1} K, respectively. Among these values, the notably negative $\Delta S^{\ddagger}$ is consistent with previous reports on C_2-type lignin model compound by Collier *et al.*[44] In their study, such highly negative $\Delta S^{\ddagger}$ values as reported in the present work have been observed only when the leaving group bears a *p*-formyl substituent. Although there are differences in substrate and OH$^-$ concentration compared to this study, the somewhat unusual $\Delta S^{\ddagger}$ associated with leaving groups containing a formyl substituent can at least partly be rationalized by the presence of side reaction pathways, which are extremely unfavorable in terms of entropy, as discussed later in this article. On the other hand, the $\Delta H^{\ddagger}$ value was approximately 5 kcal mol^{-1} lower than the reported value of 19.6 kcal mol^{-1} in that study. This discrepancy can be explained by structural differences between the model compounds, namely C_3- and C_2-side-chain, as discussed in the next section.

The E_a, $\Delta H^{\ddagger}$, $\Delta S^{\ddagger}$ for the vanillin formation reaction represented by k_1 (Route I in Scheme 2) were 17.0 kcal mol^{-1},

16.4 kcal mol^{-1}, and −26.6 cal mol^{-1} K, respectively. Compared to the corresponding values for the side reaction represented by k_2, the E_a and $\Delta H^{\ddagger}$ values for vanillin formation were approximately 3 kcal mol^{-1} higher, while $\Delta S^{\ddagger}$ was about 8 cal mol^{-1} K greater. These results clearly indicate that the vanillin formation reaction (Route I) is enthalpically less favorable but entropically more favorable than the side reaction (Route II). This implies that the entropic advantage of Route I becomes more pronounced at higher temperatures, which corresponds well with the trend observed in Table 1, where the vanillin yield increases with increasing temperature. The activation free energy ($\Delta G^{\ddagger}$), which reflects both enthalpic and entropic contributions, was calculated to be 24.3 kcal mol^{-1} for vanillin formation and 23.9 kcal mol^{-1} for the side reaction under standard conditions. The slightly higher $\Delta G^{\ddagger}$ value for vanillin formation is consistent with the observation that the rate of vanillin formation is lower than that of the side reaction. The differences in the values of the activation parameters between Route I and Route II undoubtedly reflect the differences in the chemical reactions proceeding along these routes. The activation parameters presented in this study will serve as important clues for further examining the detailed reaction mechanisms, particularly those of the side reactions whose actual nature remains unclear at present.

In principle, the $\Delta G^{\ddagger}$ value derived from k_T, which reflects the overall reaction, should fall between the two values derived from k_1 and k_2. However, as summarized in Table 2, the calculated value was slightly lower than either, at 23.7 kcal mol^{-1}. This discrepancy is likely due to error associated with the precision of the Arrhenius plot, particularly in the estimation of $\Delta S^{\ddagger}$, where the intercept of the plot is highly sensitive to experimental uncertainties in rate measurements. In any case, the three plots shown in Fig. 2 clearly reflect the trends in the slopes and intercepts of their respective regression lines. Hence, the enthalpic and entropic advantages and disadvantages of Routes I and II, as discussed above, are not undermined by this small deviation.

Quantum chemical calculations

In the previous section, various activation parameters for the vanillin formation reaction (Route I, Scheme 2) were evaluated, as summarized in Table 2. The next question of interest is the reaction mechanism by which vanillin is eliminated from the SMs. As discussed in the introduction, two possible mechanisms have been proposed for this reaction: the $S_N$icB mechanism and the S_NAr mechanism (Scheme 3). In this section, we conducted a mechanistic analysis using theoretical calculations to clarify which of these two mechanisms is operative. Previous reports on the activation barrier for vanillin formation using C_2 side-chain model compounds were carried out under conditions in which the presence of side reaction was not considered, and therefore did not isolate the activation barrier of the vanillin formation reaction itself.[44] In contrast, the activation barrier for the vanillin formation reaction, excluding the influence of side reaction (Route II), is revealed here for the first time. A rational mechanistic discussion of the vanillin
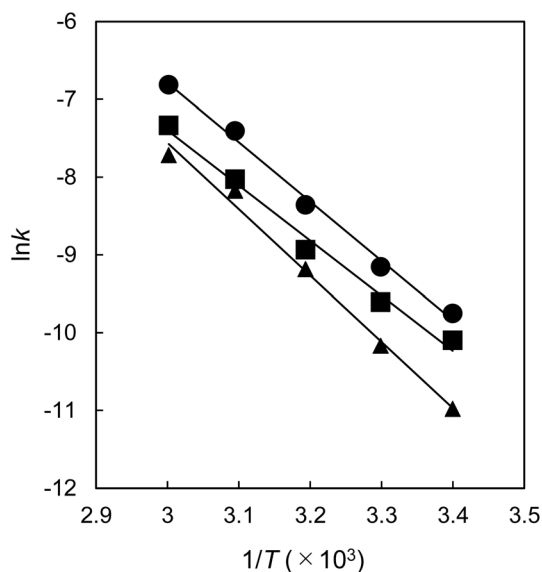

Fig. 2 Arrhenius plots constructed based on the disappearance rate of SMs (k_T) (●), the formation rate of vanillin (k_1) (▲), and the rate of side reactions (k_2) (■). For details on the calculation methods of each rate constant, see the Experimental section. The degradation experiments of SMs were performed in 4.0 mol L^{-1} NaOH aq. at 21–60 °C under N$_2$.

formation reaction thus became possible only on the basis of the kinetic analysis presented in this study.

In our quantum chemical calculations, a truncated model compound, $VE_\beta(C_2)$, was employed in place of VE_β, in which the γ-position was removed to reduce computational cost (see Scheme S1). The $S_N$icB-type elimination of a vanillin molecule from the oxyanion form of $VE_\beta(C_2)$ ($VE_\beta(C_2)^-$) was investigated at the DFT(M06-2X) level. As shown in Fig. 3, a reaction pathway was identified in which $VE_\beta(C_2)^-$ proceeds via a transition state (**TS1**) to give a product complex (**Pc**) composed of a vanillate ion and an epoxide intermediate. In this process, the distance between the α-oxygen atom (O_α) and the β-carbon atom (C_β) is progressively shortened ($2.37 \rightarrow 1.87 \rightarrow 1.43$ Å), whereas the bond between C_β and the oxygen atom of the vanillin residue (O_β) is elongated ($1.44 \rightarrow 1.91 \rightarrow 2.37$ Å), reflecting the progress

of vanillin elimination. In addition, the O_α–C_α–C_β bond angle decreases markedly from 108.7° to 58.9°, which is associated with epoxide ring formation. At the DFT(M06-2X)/BS-II level, the calculated activation Gibbs energy ($\Delta G^{0\ddagger}$) and activation energy (E_a) for this reaction were both 20.7 kcal mol^{-1}. The ΔG^0 and ΔE for the formation of **Pc** were calculated to be -7.7 and -7.0 kcal mol^{-1}, respectively, indicating that the reaction is exothermic. The structure of $VE_\beta(C_2)^-$ shown in Fig. 3 corresponds to the most stable among several possible rotamers of $VE_\beta(C_2)^-$. This structure was used as the zero-point reference for all subsequent energy evaluations, including the analysis of the acetal intermediate formation described later (for the structures of less stable rotamers, see Fig. S4 in the SI).

We next investigated the initial reaction step involving the migration of the vanillin residue in $VE_\beta(C_2)^-$, specifically the
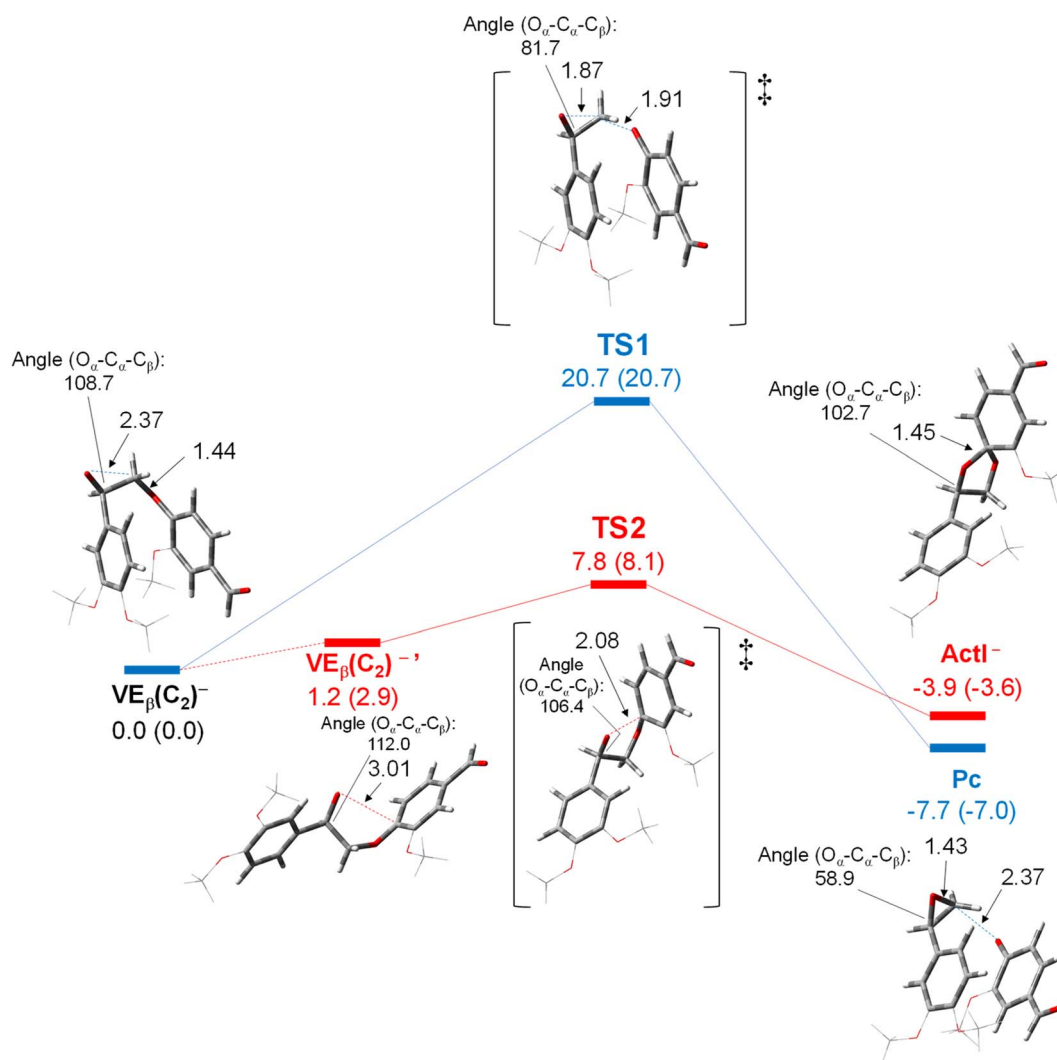

Fig. 3 Energy profile for vanillin elimination and acetal formation from $VE_\beta(C_2)^-$, calculated at the DFT(M06-2X)/BS-II//DFT(M06-2X)/BS-I level of theory. The most stable conformer of $VE_\beta(C_2)^-$ was used as the reference point (ground zero) for energy evaluation among the various possible conformers (see Fig. S4 for less stable conformers). Relative Gibbs energies (ΔG^0, in kcal mol^{-1}) are shown outside the parentheses, and the corresponding potential energies (ΔE) are given in parentheses. Atomic distances, bond angles and energies are given in Å, degrees, and kcal mol^{-1}, respectively. A reaction scheme based on structural formulas is also provided as supplementary information in the SI (see Scheme S1).

formation of an acetal intermediate. In this reaction, a rotamer of $VE_\beta(C_2)^-$, designated $VE_\beta(C_2)^{-\prime}$, which is 1.2–2.9 kcal mol^{-1} less stable than $VE_\beta(C_2)^-$ on the potential energy surface, is formed. From this rotamer, the acetal intermediate $ActI^-$ is generated *via* the transition state $TS2$. In this process, the O_α–C_4 (vanillin) bond distance is progressively shortened from 3.01 Å in $VE_\beta(C_2)^{-\prime}$ to 2.08 Å in $TS2$ and 1.45 Å in $ActI^-$, reflecting the formation of a new C–O bond. Meanwhile, the O_α–C_α–C_β bond angle decreases only slightly (112.0° → 106.4° → 102.7°), indicating that the five-membered acetal ring is formed without large angular strain, which is consistent with the relatively low activation barrier for this reaction. At the DFT(M06-2X)/BS-II level, the $\Delta G^{0\ddagger}$ (E_a) for this reaction were calculated to be 6.6 and 5.2 kcal mol^{-1}, respectively. When evaluated with reference to $VE_\beta(C_2)^-$, the $\Delta G^{0\ddagger}$ (E_a) values become 7.8 and 8.1 kcal mol^{-1}, which are more appropriate for comparison with the experimental results. These values are significantly lower than those of the vanillin elimination reaction proceeding *via* $TS1$. This result is consistent with experimental observations, in which the migration products such as VE_α and VE_γ are readily obtained simply by dissolving VE_β in aqueous alkali at room temperature,[42] whereas the formation of vanillin requires prolonged reaction times and/or heating. Note that the ΔG^0 (ΔE) for the formation of $ActI^-$ were calculated to be −3.9 (−3.6) kcal mol^{-1}, respectively, indicating that $ActI^-$ is thermodynamically more stable than $VE_\beta(C_2)^-$. At first glance, this result may appear inconsistent with experimental observations; however, this discrepancy arises from the fact that all chemical species were modeled as oxyanions in the theoretical calculations (for further discussion, see Fig. S5 and the accompanying explanation). In any case, this issue is unlikely to significantly affect the comparative evaluation of the S_NicB and S_NAr mechanisms, which is discussed below.

In this study, we did not perform direct quantum chemical calculations for the S_NAr mechanism. This is because accurate modeling of this pathway, which involves OH$^-$, would require consideration of OH$^-$ cluster formation in aqueous solution, a task that would demand substantial computational resources. Nevertheless, based on the above results for $ActI^-$ formation, it is still possible to make a rational inference regarding the S_NAr pathway. Specifically, the nucleophilic attack by OH$^-$ on the C_4 position of the vanillin residue, which initiates the S_NAr mechanism, is essentially analogous to the nucleophilic attack by an oxyanion that leads to $ActI^-$ formation. Thus, it can be reasonably expected that the E_a for the S_NAr mechanism would be similar to that of the $TS2$-mediated $ActI^-$ formation, *i.e.*, less than 10 kcal mol^{-1}. On the other hand, as discussed in Table 2, the experimentally determined E_a for vanillin formation is 17.0 kcal mol^{-1}, which is close to the value of 20.7 kcal mol^{-1} calculated for the S_NicB mechanism. It is therefore reasonable to conclude that vanillin elimination from VE_β proceeds predominantly *via* the S_NicB mechanism. The slightly lower experimental E_a compared to the calculated value may suggest a minor contribution from the S_NAr mechanism to the overall vanillin elimination process. It may also be the case that the use of the C_2-side-chain model in the calculations is another reason for such a small difference in E_a. In other words, since the three-

membered ring strain of the C_2-side-chain epoxy intermediate is greater than that of the C_3-side-chain counterpart, the E_a value is expected to be higher for $VE_\beta(C_2)$. In fact, the E_a value calculated for $VE_\beta(C_2)$ (20.7 kcal mol^{-1}, Fig. 3) is in good agreement with the experimental value reported for the same C_2-side-chain model (19.6 kcal mol^{-1}, see Table 2), although not accounting for the presence of side reaction pathways there.[44]

Although no definitive evidence currently exists to explain why vanillin elimination *via* the S_NAr mechanism—which is expected to have a lower activation energy than the S_NicB pathway—does not readily proceed, several plausible explanations can be considered. One possible explanation lies in the fact that the nucleophilic attack by OH$^-$ on the C_4 position of the vanillin moiety is a bimolecular process, which is entropically much less favorable than the intramolecular S_NicB reaction. While it is difficult to accurately compute the activation entropy for such nucleophilic attacks and thus quantify the entropic penalty, this factor may substantially elevate the true activation barrier of the S_NAr pathway. Another factor concerns the nature of the hemiacetal intermediate I_{HA}, which is required for the S_NAr mechanism to proceed, as illustrated in Scheme 6. A second possible explanation is related to the anticipated reactivity of this I_{HA}. The potential reaction pathways from I_{HA} include: formation of vanillin *via* elimination of an alkoxide group (Path A); the reverse reaction in which OH$^-$ is eliminated, regenerating the starting material (Path B); and elimination of the vanillate ion from a dianion that is formed by deprotonation of the hydroxyl group at the C_4 position (Path C). Between Path A and Path B, the latter is generally considered more favorable, as alkoxides are typically poorer leaving groups than OH$^-$. In Path C, although the second step—the elimination of the vanillate ion—is favorable, the first step—the formation of the dianion—
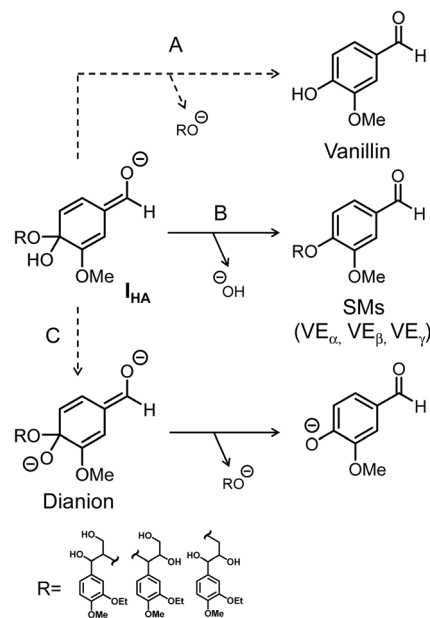
Scheme 6 Possible reaction pathways proceeding from the hemiacetal intermediate I_{HA} produced by the nucleophilic attack of OH$^-$ on the vanillin residue of the starting materials, SMs.

is highly unfavorable from both enthalpic and entropic perspectives. Therefore, even if the nucleophilic attack by OH^- at the C_4 carbon proceeds and leads to the formation of I_{HA}, the reaction is likely to revert through Path B, thereby suppressing the formation of vanillin. In any case, these considerations require further experimental and theoretical validation.

The results of this study suggest that vanillin elimination from VE_β proceeds predominantly *via* the $S_N$icB mechanism. This conclusion is further supported by the experimental observation that the yield of **ArG**, which is produced alongside vanillin in the degradation of VE_β, was consistently lower than that of vanillin under all temperature conditions (Table 1). If vanillin elimination were to proceed *via* the S_NAr mechanism, it would be expected that both vanillin and **ArG** would be generated directly from I_{HA} in a 1 : 1 molar ratio. However, this prediction clearly contradicts the experimental findings. In contrast, under the $S_N$icB mechanism, the formation of **ArG** requires nucleophilic attack by OH^- on the epoxide intermediate. Thus, the yield of **ArG** would depend on the selectivity between this nucleophilic addition and other competing side reaction, meaning that **ArG** and vanillin would not necessarily be produced in equimolar amounts. Indeed, it has been reported that, in addition to OH^- addition, the epoxide intermediate can undergo competing reactions such as deprotonation at the γ-position leading to carbonyl compound formation.[43] These considerations further support, from another standpoint, that vanillin elimination from VE_β proceeds mainly *via* the $S_N$icB mechanism.

Conclusions

In this study, we investigated the degradation mechanism of the vanillin end group model compound VE_β in 4.0 mol L^{-1} NaOH aqueous solution, with a particular focus on the vanillin elimination pathway, through both kinetic analysis and theoretical calculations. Upon dissolution in the reaction medium at room temperature, VE_β underwent terminal group transfer, forming an equilibrium mixture of starting materials (SMs) consisting of VE_α and VE_γ. The degradation of SMs was found to proceed according to the pseudo-first-order competitive reaction model shown in Scheme 4. Kinetic analysis based on this model estimated the activation energy (E_a) for vanillin formation (Route I, Scheme 2) to be 17.0 kcal mol^{-1}. This value closely matches the E_a of 20.7 kcal mol^{-1} calculated for the $S_N$icB mechanism at the DFT(M06-2X) level, suggesting that under the reaction conditions employed in this study, the elimination of vanillin predominantly proceeds *via* the $S_N$icB pathway.

In contrast, the formation pathway of high-molecular-weight components (Route II, Scheme 2), which proceeds as a side reaction of vanillin production, exhibited a reaction rate comparable to that of vanillin elimination. Although this reaction was enthalpically more favorable than the vanillin elimination reaction, it was entropically less favorable. Despite yielding relatively high-molecular-weight components as final products, this side reaction followed first-order kinetics with respect to the concentration of the SMs, strongly suggesting that its rate-determining step is unimolecular. While the detailed

molecular mechanism of this reaction remains unclear at present, these findings provide important insights toward its elucidation.

The ultimate goal of our study is to propose a kinetics-based rational strategy for controlling the vanillin-forming reaction and its associated side reactions. The findings obtained in this work reveal the reaction mechanism of vanillin formation and the kinetic characteristics of the side reaction pathways that should be suppressed. On the other hand, the specific features of these side reaction pathways, such as the chemical structure of intermediate **I**, remain unresolved, and thus, at present, it is difficult to make concrete proposals for controlling the vanillin production process. In the future, a better understanding of the molecular mechanism of this side reaction is expected to enable the development of rational strategies to suppress the competing pathway and to improve the efficiency of vanillin elimination.

Author contributions

Yuki Hirano: methodology, data curation, investigation, writing – original draft, visualization, formal analysis, funding acquisition. Haruhiko Fukaya: writing – review & editing, supervision, resources, validation. Tsunehisa Miki: writing – review & editing, resources. Takashi Hosoya: conceptualization, writing – review & editing, supervision, project administration, funding acquisition, validation. Hisashi Miyafuji: writing – review & editing, supervision, funding acquisition, validation.

Conflicts of interest

The authors declare no competing financial or personal interests.

Data availability

Data for this study, including figures and tables, are available within the article. The data supporting this article have also been included as part of the supplementary information (SI). Supplementary information is available. See DOI: https://doi.org/10.1039/d5ra05285h.

References

1 J. Ralph, G. Brunow, and W. Boerjan, *Lignins, Encyclopedia of Life Sciences (eLS)*, John Wiley & Sons, Ltd., Chichester, 2007, DOI: **10.1002/9780470015902.a0020104**.

2 M. Fache, B. Boutevin and S. Caillol, Vanillin Production from Lignin and Its Use as a Renewable Chemical, *ACS Sustainable Chem. Eng.*, 2016, **4**(1), 35–46, DOI: **10.1021/acssuschemeng.5b01344**.

3 S. Gillet, M. Aguedo, L. Petitjean, A. R. C. Morais, A. M. da Costa Lopes, R. M. Łukasik and P. T. Anastas, Lignin Transformation for High Value Applications: Towards Targeted Modifications Using Green Chemistry, *Green Chem.*, 2017, **19**, 4200–4233, DOI: **10.1039/C7GC01479A**.

4 Y. Jing, L. Dong, Y. Guo, X. Liu and Y. Wang, Chemicals from Lignin: A Review of the Catalytic Conversion Involving Hydrogen, *ChemSusChem*, 2020, **13**(17), 4181–4198, DOI: **10.1002/cssc.201903174**.

5 H. Kawamoto, Lignin Pyrolysis Reactions, *J. Wood Sci.*, 2017, **63**, 117–132, DOI: **10.1007/s10086-016-1606-z**.

6 C. Li, X. Zhao, A. Wang, G. W. Huber and T. Zhang, Catalytic Transformation of Lignin for the Production of Chemicals and Fuels, *Chem. Rev.*, 2015, **115**(21), 11559–11624, DOI: **10.1021/acs.chemrev.5b00155**.

7 X. Liu, F. P. Bouxin, J. Fan, V. L. Budarin, C. Hu and J. H. Clark, Recent Advances in the Catalytic Depolymerization of Lignin towards Phenolic Chemicals: A Review, *ChemSusChem*, 2020, **13**(17), 4296–4317, DOI: **10.1002/cssc.202001213**.

8 R. Ma, Y. Xu and X. Zhang, Catalytic Oxidation of Biorefinery Lignin to Value-added Chemicals to Support Sustainable Biofuel Production, *ChemSusChem*, 2014, **8**(1), 24–51, DOI: **10.1002/cssc.201402503**.

9 R. Rinaldi, R. Jastrzebski, M. T. Clough, J. Ralph, M. Kennema, P. C. A. Bruijnincx and B. M. Weckhuysen, Paving the Way for Lignin Valorisation: Recent Advances in Bioengineering, Biorefining and Catalysis, *Angew. Chem., Int. Ed.*, 2016, **55**(29), 8164–8215, DOI: **10.1002/anie.201510351**.

10 P. C. R. Pinto, E. A. B. da Silva, and A. E. Rodrigues, *Lignin as Source of Fine Chemicals: Vanillin and Syringaldehyde. Biomass Conversion*, 2012, pp. 381–420.

11 A. More, T. Elder and Z. Jiang, Towards a New Understanding of the Retro-Aldol Reaction for Oxidative Conversion of Lignin to Aromatic Aldehydes and Acids, *Int. J. Biol. Macromol.*, 2021, **183**, 1505–1513, DOI: **10.1016/j.ijbiomac.2021.05.100**.

12 Y. Zhu, Y. Liao, W. Lv, J. Liu, X. Song, L. Chen, C. Wang, B. F. Sels and L. Ma, Complementing Vanillin and Cellulose Production by Oxidation of Lignocellulose with Stirring Control, *ACS Sustainable Chem. Eng.*, 2020, **8**(6), 2361–2374, DOI: **10.1021/acssuschemeng.9b04837**.

13 Y. Wang, S. Sun, F. Li, X. Cao and R. Sun, Production of Vanillin from Lignin: The Relationship Between β-O-4 Linkages and Vanillin Yield, *Ind. Crops Prod.*, 2018, **116**, 116–121, DOI: **10.1016/j.indcrop.2018.02.043**.

14 V. E. Tarabanko, K. L. Kaygorodov, D. O. Vigul, N. Tarabanko, Y. V. Chelbina and M. A. Smirnova, Influence of Acid Prehydrolysis on the Process of Wood Oxidation into Vanillin and Pulp, *J. Wood Chem. Technol.*, 2020, **40**(6), 421–433, DOI: **10.1080/02773813.2020.1835984**.

15 S. Rawat, P. Gupta, B. Singh, T. Bhaskar, K. Natte and A. Narani, Molybdenum-Catalyzed Oxidative Depolymerization of Alkali Lignin: Selective Production of Vanillin, *Appl. Catal., A*, 2020, **598**, 117567, DOI: **10.1016/j.apcata.2020.117567**.

16 H. Paananen, E. Eronen, M. Mäkinen, J. Jänis, M. Suvanto and T. T. Pakkanen, Base-Catalyzed Oxidative Depolymerization of Softwood Kraft Lignin, *Ind. Crops Prod.*, 2020, **152**, 112473, DOI: **10.1016/j.indcrop.2020.112473**.

17 O. Y. Abdelaziz, K. Ravi, F. Mittermeier, S. Meier, A. Riisager, G. Lidén and C. P. Hulteberg, Oxidative Depolymerization of Kraft Lignin for Microbial Conversion, *ACS Sustainable Chem. Eng.*, 2019, **7**(13), 11640–11652, DOI: **10.1021/acssuschemeng.9b01605**.

18 W. Schutyser, T. Renders, S. Van den Bosch, S.-F. Koelewijn, G. T. Beckham and B. F. Sels, Chemicals from Lignin: an Interplay of Lignocellulose Fractionation, Depolymerisation, and Upgrading, *Chem. Soc. Rev.*, 2018, **47**(3), 852–908, DOI: **10.1039/C7CS00566K**.

19 M. Maeda, T. Hosoya, K. Yoshioka, H. Miyafuji, H. Ohno and T. Yamada, Vanillin Production from Native Softwood Lignin in the Presence of Tetrabutylammonium Ion, *J. Wood Sci.*, 2018, **64**, 810–815, DOI: **10.1007/s10086-018-1766-0**.

20 T. Hosoya, D. Okamoto, H. Miyafuji and T. Yamada, Production of Vanillin and Vanillic Acid by Aerobic Oxidation of Polyethylene Glycol (PEG)-modified Glycol Lignin in Tetrabutylammonium Hydroxide, *Lignin*, 2021, **2**, 9–18, DOI: **10.62840/lignin.2.0_9**.

21 G. Lyu, C. G. Yoo and X. Pan, Alkaline Oxidative Cracking for Effective Depolymerization of Biorefining Lignin to Mono-aromatic Compounds and Organic Acids with Molecular Oxygen, *Biomass Bioenergy*, 2018, **108**, 7–14, DOI: **10.1016/j.biombioe.2017.10.046**.

22 P. Ding, M. Garrett, Ø. Loe, A. W. Nienow and A. W. Pacek, Generation of Hydrogen Gas during the Catalytic Oxidation of Sodium Lignosulfonate to Vanillin: Initial Results, *Ind. Eng. Chem. Res.*, 2012, **51**(1), 184–188, DOI: **10.1021/ie201607t**.

23 H. Zhang, X. Yong, J. Zhou, J. Deng and Y. Wu, Biomass Vanillin-Derived Polymeric Microspheres Containing Functional Aldehyde Groups: Preparation, Characterization, and Application as Adsorbent, *ACS Appl. Mater. Interfaces*, 2016, **8**(4), 2753–2763, DOI: **10.1021/acsami.5b11042**.

24 R. Ciriminna, A. Fidalgo, F. Meneguzzo, F. Parrino, L. M. Ilharco and M. Pagliaro, Vanillin: The Case for Greener Production Driven by Sustainability Megatrend, *ChemistryOpen*, 2019, **8**(6), 660–667, DOI: **10.1002/open.201900083**.

25 H.-R. Bjørsvik and F. Minisci, Fine Chemicals from Lignosulfonates. 1. Synthesis of Vanillin by Oxidation of Lignosulfonates, *Org. Process Res. Dev.*, 1999, **3**(5), 330–340, DOI: **10.1021/op9900028**.

26 R. Behling, S. Valange and G. Chatel, Heterogeneous Catalytic Oxidation for Lignin Valorization into Valuable Chemicals: What results? What limitations? What trends?, *Green Chem.*, 2016, **18**(7), 1839–1854, DOI: **10.1039/C5GC03061G**.

27 W. Jeon, I. Choi, J. Park, J. Lee and K. Hwang, Alkaline Wet Oxidation of Lignin over Cu-Mn Mixed Oxide Catalysts for Production of Vanillin, *Catal. Today*, 2020, **352**, 95–103, DOI: **10.1016/j.cattod.2019.12.037**.

28 K. Yamamoto, T. Hosoya, K. Yoshida, H. Miyafuji, H. Ohno and T. Yamada, Tetrabutylammonium Hydroxide 30-Hydrate as Novel Reaction Medium for Lignin Conversion, *ACS Sustain. Chem. Eng.*, 2017, **5**(11), 10111–10115, DOI: **10.1021/acssuschemeng.7b02106**.

29 A. W. Pacek, P. Ding, M. Garrett, G. Sheldrake and A. W. Nienow, Catalytic Conversion of Sodium Lignosulfonate to Vanillin: Engineering Aspects. Part 1. Effects of Processing Conditions on Vanillin Yield and Selectivity, *Ind. Eng. Chem. Res.*, 2013, **52**(25), 8361–8372, DOI: **10.1021/ie4007744**.

30 V. E. Tarabanko, D. V. Petukhov and G. E. Selyutin, New Mechanism for the Catalytic Oxidation of Lignin to Vanillin, *Kinet. Catal.*, 2004, **45**(4), 569–577, DOI: **10.1023/B:KICA.0000038087.95130.a5**.

31 J. D. P. Araújo, C. A. Grande and A. E. Rodrigues, Vanillin Production from Lignin Oxidation in a Batch Reactor, *Chem. Eng. Res. Des.*, 2010, **88**(8), 1024–1032, DOI: **10.1016/j.cherd.2010.01.021**.

32 E. A. B. da Silva, M. Zabkova, J. D. Araújo, C. A. Cateto, M. F. Barreiro, M. N. Belgacem and A. E. Rodrigues, An Integrated Process to Produce Vanillin and Lignin-Based Polyurethanes from Kraft Lignin, *Chem. Eng. Res. Des.*, 2009, **87**(9), 1276–1292, DOI: **10.1016/j.cherd.2009.05.008**.

33 J. Gierer and I. Pettersson, Stusied on Condensation of Lognins in Alkaline Media. 2. Formation of Stilbene and Arylcoumaran Sturucures through Neighboring Group Participation Reactions, *Can. J. Chem.*, 1977, **55**(4), 593–599, DOI: **10.1139/v77-084**.

34 G. Gellerstedt and R. Agnemo, The Reactions of Lignin with Alkaline Hydrogen Peroxide. Part III. The Oxidation of Conjugated Carbonyl Structures, *Acta Chem. Scand.*, 1980, **34**, 275–280, DOI: **10.3891/acta.chem.scand.34b-0275**.

35 J. Gierer, Chemistry of Delignification, *Wood Sci. Technol.*, 1986, **20**(1), 1–33, DOI: **10.1007/BF00350692**.

36 T. Yokoyama, I. Maekawa, Y. Matsumoto and G. Meshitsuka, Reaction Selectivity of Active Oxygen Species Produced by Oxygen–Alkali Oxidation of a Phenolic Compound, *J. Wood Sci.*, 1998, **44**(5), 421–422, DOI: **10.1007/BF01130459**.

37 S. Shimizu, P. Posoknistakul, T. Akiyama, T. Yokoyama and Y. Matsumoto, Effects of Aromatic Ring Type on Reactions Subsequent to the β-O-4 Bond Cleavage of Non-Phenolic Lignin Model Compounds under Alkaline Pulping Conditions, *J. Wood Sci.*, 2018, **64**(5), 664–674, DOI: **10.1007/s10086-018-1739-3**.

38 S. Ohmura, T. Yokoyama and Y. Matsumoto, Significance of Benzylic Hydroxymethylene Group in the Reaction of Lignin Side-Chain with Active Oxygen Species under Oxygen Bleaching Conditions, *J. Wood Sci.*, 2013, **59**, 337–343, DOI: **10.1007/s10086-013-1339-1**.

39 T. Hosoya, K. Kawase, Y. Hirano, M. Ikeuchi and H. Miyafuji, Alkaline Aerobic Oxidation of Native Softwood Lignin in the Presence of Na+−Cyclic Polyether Complexes, *J. Wood Chem. Technol.*, 2022, **42**(1), 1–14, DOI: **10.1080/02773813.2021.1998127**.

40 T. Hosoya, K. Yamamoto, H. Miyafuji and T. Yamada, Selective Production of Bio-Based Aromatics by Aerobic Oxidation of Native Softwood Lignin in Tetrabutylammonium Hydroxide, *RSC Adv.*, 2020, **10**, 19199–19210, DOI: **10.1039/d0ra03420g**.

41 Y. Hirano, T. Hosoya, and H. Miyafuji, Depolymerization of Native Lignin into Vanillin, Vanillic Acid, and Other Related Compounds via Alkaline Aerobic Oxidation: Reaction Mechanisms and Process Control Using Organic Cations, *From Biomass to Biobased Products*, 2023, Chapter 9, DOI: **10.5772/intechopen.107581**.

42 Y. Hirano, T. Hosoya and H. Miyafuji, Alkaline-Induced Degradation Pathways of β-O-4-Linked Vanillin Moieties Produced During Lignin Oxidation and the Effect of Na+-Cyclic Polyether Complexes, *ACS Omega*, 2025, **10**(35), 40646–40657, DOI: **10.1021/acsomega.5c07658**.

43 Y. Kato, S. Shimizu, T. Akiyama, T. Yokoyama and Y. Matsumoto, Effect of Counter Cation on Alkaline Reaction of β-O-4-Type Substructure in Lignin, *J. Wood Chem. Technol.*, 2019, **39**(2), 111–123, DOI: **10.1080/02773813.2018.1508302**.

44 W. E. Collier, T. H. Fisher, L. L. Ingram Jr, A. L. Harris and T. P. Schultz, Alkaline Hydrolysis of Nonphenolic β-O-4 Lignin Model Dimers: Further Studies of the Substituent Effect on the Leaving Phenoxide, *Holzforschung*, 1996, **50**(5), 420–424, DOI: **10.1515/hfsg.1996.50.5.420**.

45 T. F. Hubbard, T. P. Schultz and T. H. Fisher, Alkaline Hydrolysis of Nonphenolic β-O-4 Lignin Model Dimers: Substituent Effects on the Leaving Phenoxide in Neighboring Group vs Direct Nucleophilic Attack, *Holzforschung*, 1992, **46**(4), 315–320, DOI: **10.1515/hfsg.1992.46.4.315**.

46 Y. Hirano, A. Izawa, T. Hosoya and H. Miyafuji, Degradation Mechanism of a Lignin Model Compound during Alkaline Aerobic Oxidation: Formation of the Vanillin Precursor from the β-O-4 Middle Unit of Softwood Lignin, *React. Chem. Eng.*, 2022, **7**, 1603–1616, DOI: **10.1039/D2RE00036A**.

47 M. J. Frisch, G. W. Trucks, H. B. Schlegel, G. E. Scuseria, M. A. Robb, J. R. Cheeseman, G. Scalmani, V. Barone, G. A. Petersson, H. Nakatsuji, X. Li, M. Caricato, A. Marenich, J. Bloino, B. G. Janesko, R. Gomperts, B. Mennucci, H. P. Hratchian, J. V. Ortiz, A. F. Izmaylov, J. L. Sonnenberg, D. Williams-Young, F. Ding, F. Lipparini, F. Egidi, J. Goings, B. Peng, A. Petrone, T. Henderson, D. Ranasinghe, V. G. Zakrzewski, J. Gao, N. Rega,

G. Zheng, W. Liang, M. Hada, M. Ehara, K. Toyota, R. Fukuda, J. Hasegawa, M. Ishida, T. Nakajima, Y. Honda, O. Kitao, H. Nakai, T. Vreven, K. Throssell, J. A. Montgomery, J. E. Peralta, F. Ogliaro, M. Bearpark, J. J. Heyd, E. Brothers, K. N. Kudin, V. N. Staroverov, T. Keith, R. Kobayashi, J. Normand, K. Raghavachari, A. Rendell, J. C. Burant, S. S. Iyengar, J. Tomasi, M. Cossi, J. M. Millam, M. Klene, C. Adamo, R. Cammi, J. W. Ochterski, R. L. Martin, K. Morokuma, O. Farkas, J. B. Foresman, and D. J. Fox, *Gaussian 09, Revision A.02*, Gaussian, Inc., Wallingford CT, 2016.

48 J. R. Obst, Kinetics of Alkaline Cleavage of β-Aryl Ether Bonds in Lignin Models: Significance to Delignification, *Holzforschung*, 1983, **37**(1), 23–28, DOI: **10.1515/hfsg.1983.37.1.23**.